ACES Asian Chemical Editorial Society

DOI: 10.1002/cnma.201700006

CHEMNANOMAT
Communication

Perovskite Nanocrystals

Facile Morphology-Controlled Synthesis of Organolead Iodide Perovskite Nanocrystals Using Binary Capping Agents

Elke Debroye,[a] Haifeng Yuan,*[a] Eva Bladt,[b] Wouter Baekelant,[a] Mark Van der Auweraer,[a] Johan Hofkens,[a, c] Sara Bals,[b] and Maarten B. J. Roeffaers*[d]

Abstract: Controlling the morphology of organolead halide perovskite crystals is crucial to a fundamental understanding of the materials and to tune their properties for device applications. Here, we report a facile solution-based method for morphology-controlled synthesis of rod-like and plate-like organolead halide perovskite nanocrystals using binary capping agents. The morphology control is likely due to an interplay between surface binding kinetics of the two capping agents at different crystal facets. By high-resolution scanning transmission electron microscopy, we show that the obtained nanocrystals are monocrystalline. Moreover, long photoluminescence decay times of the nanocrystals indicate long charge diffusion lengths and low trap/defect densities. Our results pave the way for large-scale solution synthesis of organolead halide perovskite nanocrystals with controlled morphology for future device applications.

Organolead halide perovskites (OHP) attract a lot of attention in the field of solar energy conversion because of their high absorption coefficient at visible wavelengths and long-range electron–hole diffusion. Planar perovskite-based photovoltaic devices consist of a thin perovskite layer, $CH_3NH_3PbX_3$ (X = Cl, Br, I), deposited between conductive scaffolds and exhibit power conversion efficiencies exceeding 20%.[1,2] The crystallinity and morphology of the perovskite layer are known to be crucial as they influence the charge carrier dynamics, conversely having a significant impact on their microscopic properties[3,4] and their device performance.[5–8] The conventional continuous perovskite films prepared by thermal annealing display large variations in grain morphology as well as in their local chemical composition. Moreover, the generally encountered high defect density in a polycrystalline film is detrimental for the charge carrier dynamics.[9–11] Potential improvement is offered by the use of monocrystalline OHP nanocrystals (NCs). Particularly, solution-processed synthesis methods yielding high-quality monocrystalline OHP crystals could form the cornerstone of fundamental studies or large-scale application in perovskite-based devices. On the one hand, the charge carrier mobility of single crystals is better than that of polycrystalline films.[12,13] On the other hand, the morphology of the crystals has a strong influence over the material properties. For instance, surfaces are known to host higher densities of traps and play important roles in determining the material properties.[3,9,14] Therefore, the surface-to-volume ratios of nanocrystals can greatly influence the trap-assisted processes in the material.

Analogous to metal and metal oxide nanoparticle formation,[15–17] oriented attachment of the capping agent to a particular facet plays an important role in controlling the morphology. Hence, anisotropic crystal growth can be promoted by forcing further delivery of precursor reagents along the perpendicular axis.[18,19] On the other hand, the ligand layer can physically block the delivery of new precursor reagents. These thermodynamic, kinetic and steric factors are widely used for synthesis of NCs with anisotropic shapes.[20,21] Likewise, the use of capping ligands is promising for crystal morphology control in OHP colloidal synthesis.

So far, there are only a few reports on ligand-assisted solution synthesis of colloidal methylammonium lead halide ($MAPbX_3$) NCs of nanowires, rods, sheets and quantum dot-like particles.[22–26] Vybornyi et al.[27] demonstrated the synthesis of $MAPbX_3$ nanocubes, nanowires and nanoplates, exclusively conducted in the nonpolar solvent 1-octadecene in the presence of oleylamine (OAm) and oleic acid (OAc). After purifica-

[a] Dr. E. Debroye, Dr. H. Yuan, W. Baekelant, Prof. Dr. M. Van der Auweraer, Prof. Dr. J. Hofkens
Department of Chemistry
KU Leuven
Celestijnenlaan 200F, B-3001, Leuven (Belgium)
E-mail: haifeng.yuan@kuleuven.be

[b] E. Bladt, Prof. Dr. S. Bals
EMAT
University of Antwerp
Groenenborgerlaan 171, B-2020, Antwerp (Belgium)

[c] Prof. Dr. J. Hofkens
RIES
Hokkaido University
N20W10, Kita-Ward, 001–0020 Sapporo (Japan)

[d] Prof. Dr. M. B. J. Roeffaers
Center for Surface Chemistry and Catalysis
KU Leuven
Celestijnenlaan 200F, B-3001, Leuven (Belgium)
E-mail: maarten.roeffaers@kuleuven.be

Supporting information for this article can be found under: http://dx.doi.org/10.1002/cnma.201700006.

tion, however, the obtained perovskite nanostructures quickly aggregated. Pathak et al.[28] and Aharon et al.[19] synthesized mixed halide OHP NCs using octylamine and OAc. In their procedure, a certain fraction of methylammonium halide was replaced by octylammonium halide, which strongly attached to the perovskite surface. Nevertheless, the existing methods often suffer from (i) strong inhomogeneity in sizes and shape of the NCs and (ii) poor stability in suspension after purification.[19,22–25,27,28]

Herein, we demonstrate morphology-controlled synthesis of $MAPbI_3$ NCs using oleic acid (OAc) and oleylamine (OAm) as capping ligands. The resulting OHP NCs are stable in suspension for a few weeks in the dark. Briefly, the lead iodide (PbI_2) and methylammonium iodide (MAI) precursor solution in acetonitrile is injected into the toluene solution containing the capping agents under vigorous stirring. Upon mixing, the solution shows an immediate color change from transparent to red, indicating formation of methyl ammonium lead iodide ($MAPbI_3$) perovskite nuclei. Further growth of these nuclei is driven by further precipitation of the precursor reagents by addition of an extra volume of toluene in a second step. After stirring for four hours, a dark brown suspension of perovskite NCs in toluene is obtained. The suspension is then centrifuged and washed with toluene to remove the excess of capping agents and unreacted precursors. This procedure is schematically represented in Figure S1 in the Supporting Information. The suspension of OHP NCs is stable for months in dark at room temperature, as revealed by scanning electron microscopy (SEM) and photoluminescence (PL) spectroscopy.

Morphology control of NCs in such a synthesis protocol is highly dependent on the ratio of the binary capping agents, but is less sensitive to the volume of toluene added in the second step or to the reaction temperature (Figure S2–S3). On the one hand, the presence of OAm is essential for guiding the anisotropic growth of NCs; it has been suggested that alkylammonium compounds interact via their amine terminal with bromide at the crystal surface of perovskite structures via [Br…H–N^+] hydrogen bridges, while the hydrocarbon tail is directed away from the surface.[29,30] It is likely that OAm has a preferred binding affinity to certain crystal facets. OAc, on the other hand, plays an important role in the OHP NCs stabilization in suspension (Figure S4). Eventually, in the non-polar toluene suspension, the final composition of the capping ligand layer is presumed to obey electrostatic neutrality. In the following sections, we investigate the impact of the binary capping agents on shape and size distribution of $MAPbI_3$ NCs by varying capping agent and precursor concentrations.

Influence of OAm and OAc amounts: For rod-like NCs, the effects of solution compositional changes were first checked by varying the amount of OAm while keeping the amounts of OAc and precursors fixed (OAc/PbI_2 mol ratio of 1, both 0.02 mmol). In these series, mainly rod-like NCs were obtained as shown in the SEM images in Figure 1 a–c. Below an OAm/PbI_2 ratio 0.75 (14.9 μmol of OAm), the average length of the rods is 400–600 nm (Figure 1 d). With higher OAm/PbI_2 ratios above 0.75, the rods become longer in their longitudinal axis (up to an average length of 2 μm). For all the tested combinations, the NC width does not change notably, ranging between 60 and 100 nm. Figure 1 d displays the correlation of nanorod aspect ratios and OAm concentrations, demonstrating direct control over the aspect ratio simply by varying OAm concentrations. This observation is most likely due to the preferential adsorption of OAm to certain crystal facets, resulting in crystal growth along the direction with lower packing density.[18,19,31] However, we can hardly identify the exact facets on which OAm has a higher binding affinity in this study. A further increase of the OAm/PbI_2 molar ratio to more than 2 does not result in higher aspect ratios. Instead, their average lengths and relative aspect ratios slightly decrease after reaching a maximum value, presumably due to steric hindrance of the ligands adsorbed to the crystal surface.

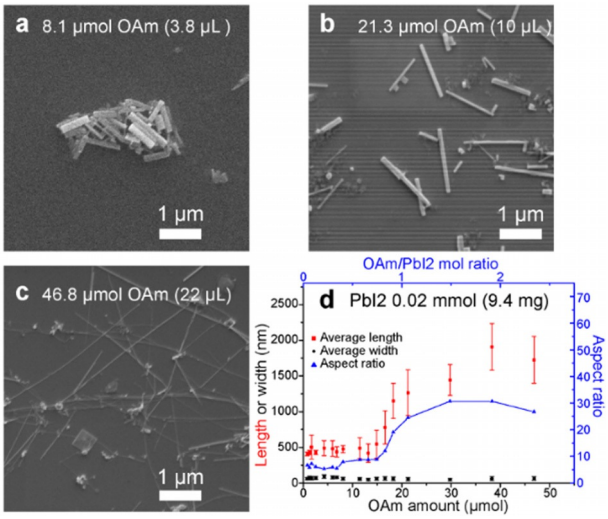

Figure 1. (a–c) Representative SEM images of $MAPbI_3$ NCs obtained after increasing the amount of OAm capping agent with a fixed molar ratio of OAc/PbI_2 1. (d) NC average dimensions and aspect ratio versus the added volume of OAm; error bars indicate the standard deviation.

In reaction mixtures with a fixed OAm/PbI_2 molar ratio of 0.33 and OAc/ PbI_2 molar ratios below 2 (8.9 μmol–23.8 μmol OAc, volume 2.8 μL–7.5 μL), rods with dimensions of 400–560 nm × 50–70 nm were obtained. Increasing the OAc amount to an OAc/ PbI_2 ratio of 6.68, the morphology shifts to smaller rods and eventually to plates.

With a lower precursor amount (PbI_2 4.7 mg, 0.01 mmol) and an increased OAc/PbI_2 molar ratio of 6.68, plate-like NCs were obtained irrespective of the amount of OAm. Increasing the OAm/PbI_2 molar ratio from 0.3 to 1.4 does not greatly influence the average lateral sizes of the plates ranging from 260 nm × 160 nm to 340 nm × 200 nm (Figure 2). Among these samples, only a 6% increase in the aspect ratio has been observed (Figure 2).

These findings clearly indicate that a prominent presence of OAc overwhelms the anisotropic growth guided by OAm, which can be explained by the strong nucleophilic nature of the ligands. Negatively charged oleic acid is supposed to form a relatively strong metal–ligand chelate when binding to the surface lead atoms of perovskite crystals.[29,32] As a result, the

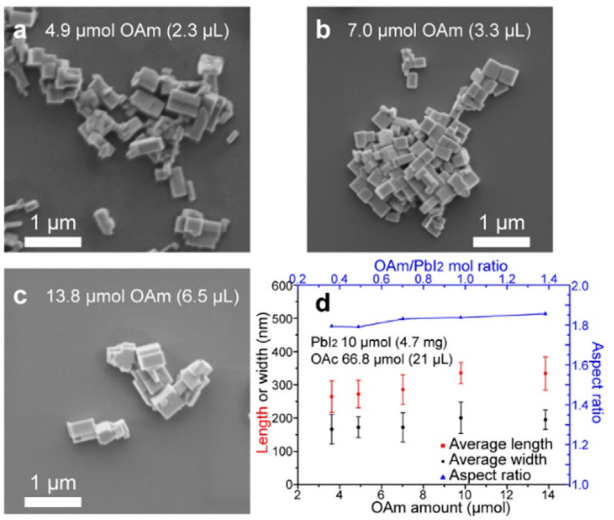

Figure 2. (a–c) Representative SEM images of $MAPbI_3$ NCs obtained after increasing the OAm concentration with a fixed molar ratio OAc/PbI_2 6.68. (d) NC average dimensions and the aspect ratio in function of the added volume of OAm; error bars indicate the standard deviation.

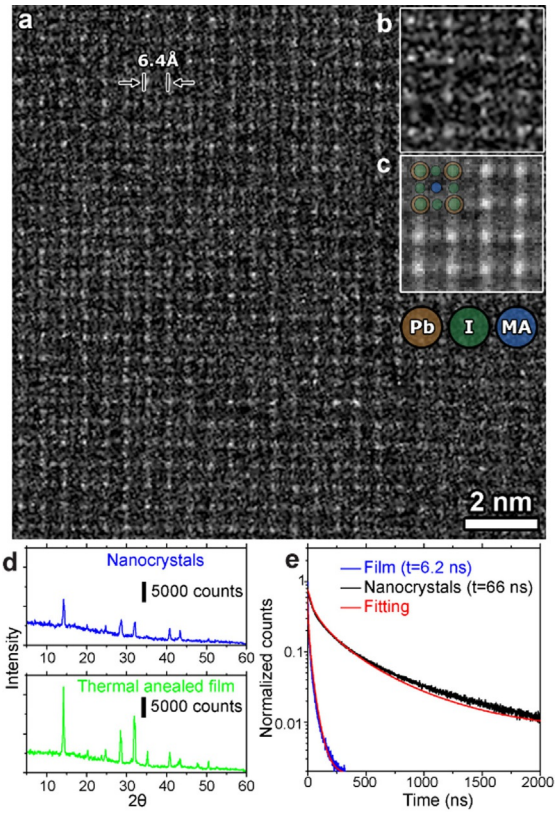

Figure 3. (a) High-resolution HAADF-STEM image of a $MAPbI_3$ NC which was acquired with a low electron dose. (b) The quality of the selected template is hampered by the low SNR. (c) After template-matching, the atomic arrangement of the NC is resolved in the averaged template. The lattice parameter is approximately 6.4 Å. (d) XRD pattern of the solution-processed perovskite NCs compared to that of a thermal annealed film. (e) PL decay times of a thermal annealed film and of the prepared $MAPbI_3$ NCs.

surface binding of OAc to OHP can be less facet selective. Thus, morphology control of OHP NCs in this synthesis method is achieved by tuning the surface binding kinetics of both capping agents, OAm and OAc.

A simultaneous increase in concentration of both capping ligands results in a slight increase in the NCs lengths (Figure S5), indicating that the molar ratio between capping agents and precursors also influences the final morphology of NCs.

Further increases in the precursor amount more than 0.02 mmol (PbI_2 9.4 mg) did not lead to larger rod-like or plate-like NCs, which is most likely due to higher nucleation rates at higher precursor concentrations. In this case, increased amounts of precursors result in broadly dispersed samples consisting of a high fraction of small-sized $MAPbI_3$ NCs and often aggregates.

It is noteworthy that the choice of solvents is also critical for the morphology control, which is also noticed by other reports.[22,25] Different solvent pairs were tested, such as dimethylformamide, dimethylsulfoxide, γ-butyrolactone. However, we found acetonitrile to yield the best morphology control with high yields, 80% for nanorods and nanowires (Figure S6), 96% for nanoplates. This is most likely due to the different polarity of the solvents.

High-resolution transmission electron microscopy (HRTEM), X-ray diffraction (XRD), and photoluminescence (PL): Besides the ability to control NC morphology in solution synthesis, the binary capping agents also help to yield high quality monocrystalline NCs, as is evident from HRTEM measurements. Figure 3a presents a high-angle annular dark field scanning transmission electron microscopy (HAADF-STEM) image of such a $MAPbI_3$ NC. As the NCs are extremely sensitive to the electron beam (Figure S9–S11),[10,22,33] a relatively low electron dose was applied, which leads to a low signal-to-noise ratio (SNR) in a single HAADF-STEM image (Figure 3a). To improve the SNR, the HAADF-STEM images are statistically averaged using a template-matching procedure, similar as that used in a previous report.[34] In this template-matching routine, specific regions are searched for in a given image that correspond to a template, which leads to an averaged template image with an improved SNR. In Figure 3b, the template is shown from which a proper analysis is hampered by the low SNR. After applying the template-matching procedure, the perovskite lattice is clearly visible in the averaged template in Figure 3c. The averaged template image shows that the synthesized NCs have a crystalline structure with a lattice parameter of approximately 6.4 Å. STEM measurements show that the synthesized nanocrystals are monocrystalline. The chemical composition can be reflected in their energy dispersive X-ray (EDX) spectroscopic data and EDX mapping results can be consulted in the Supporting Information, Figures S9 and S10.

A typical bulk XRD pattern of the synthesized OHP NCs is shown in the upper panel of Figure 3d, which resembles that of a thermal annealed film depicted in the lower panel.

PL of OHP NCs is an indication for local charge dynamics, and thus for the crystal quality.[9,12,13,35] PL decay of NCs can be well-fitted with a stretched exponential function with a characteristic time of 66 ns, as depicted in Figure 3e. This value is 10

times larger than that typically obtained for polycrystalline films (6.2 ns). The longer decay times indicate longer charge carrier diffusion lengths and thus lower trap/defect densities. Repeated SEM, XRD and PL measurements have shown that the crystals in suspension remained stable for months when stored in dark at room temperature (Figure S12 and S13).

In summary, we have demonstrated a facile two-step all-solution synthesis of $MAPbI_3$ NC with controllable morphology by employing the binary capping agents OAm and OAc. In this study, we systematically investigated the role of OAm and OAc in controlling NCs morphology. By varying the molar ratios of both capping agents, rod-like and plate-like NCs can be synthesized. The morphology and dimensions of OHP nanoparticles is likely dominated by the interplay of capping ligands coordinating to specific crystal facets. However, it is difficult to conclude the exact mechanism due to lack of knowledge in the facet-specific binding of capping ligands, the two capping agents' mutually interaction and to which extent the particle is screened from its solution environment. Further studies on OHP NCs surface interactions with capping ligands and other binary agent combinations are necessary for an improved understanding to further rationalize OHP NC synthesis procedures. This study unravels a novel approach using binary capping agents to control the morphology of high-quality and stable monocrystalline OHP NCs in suspension. The presented method paves the way for high-yield large-scale colloidal monocrystalline OHP synthesis for future fabrication of perovskite-based devices with a notably decreased defect density and subsequent higher quality.

While finalizing the manuscript, a paper by Levchuk et al. reported a similar synthesis protocol for thickness modulation of perovskite nanoplatelets using the same ligand combination but with much high concentrations, leading to nanoplatelets about 10 nm in dimension with tunable thickness.[25] We note that in that report a high ratio between OAc and OAm of 200 μL/30 μL or 200 μL/60 μL were applied to yield nanoplatelets,[25] in good agreement with our report here (the OAc/OAm ratio of 6.68 for plate-like nanocrystals).

Experimental Section

To produce perovskite NCs, the injection–precipitation method was used.

The precursor solution was prepared by dissolving lead iodide (PbI_2, 0.02 mmol, 9.4 mg) and methylammonium iodide (CH_3NH_3I, 0.06 mmol, 9.4 mg) in 10 mL of acetonitrile (ACN). In a second vial, the capping agents oleic acid (OAc) and oleylamine (OAm) were dissolved in toluene as non-solvent for the precursor reagents. Amounts used ranged between 8.9 μmol (2.8 μL) and 66.8 μmol (21 μL) for OAc, 0.85 μmol (0.4 μL) and 46.8 μmol (22 μL) for OAm and around 5 mL for toluene.

Five minutes after injection of 1.3 mL of the precursor solution to the vigorously stirred capping agent solution, a second volume of toluene ranging from 4 to 10 mL was added dropwise. The mixture was kept stirring at room temperature for four hours, resulting in a dark brown suspension containing nanoscale perovskite crystals. The dark brownish suspension was then washed and redispersed in 4 mL of toluene twice by centrifugation for 30 minutes at 4200 rpm. The final suspension was maintained in the dark. The nanocrystals in a solid phase show a photoluminescence quantum yield of about 0.84% (Figure S14). The photoluminescence quantum yields (QY) were recorded on an Edinburgh FLS980 fluorimeter, which was been extended with an external integrated sphere from Labsphere connected to the fluorimeter via optical fibers (see Figure S14). The sample was drop-casted on a quartz plate prior to the measurement. Scattering of the excitation beam by the sample was compared to a barium sulfate sample that was used as reference, which has almost complete reflectance. The QY was determined at 488 nm excitation using a similar approach as the one described in a previous report.[36]

Acknowledgements

We acknowledge financial support from the Research Foundation-Flanders (FWO, grant G.0197.11, G.0962.13, G0B39.15, postdoctoral fellowship to E.D. and H.Y.), KU Leuven Research Fund (C14/15/053), the Flemish government through long term structural funding Methusalem (CASAS2, Meth/15/04), the Hercules foundation (HER/11/14), the Belgian Federal Science Policy Office (IAP-PH05), the EC through the Marie Curie ITN project iSwitch (GA-642196) and the ERC project LIGHT (GA-307523). S.B. acknowledges financial support from European Research Council (ERC Starting Grant #335078-COLOURATOMS). E.B. gratefully acknowledges financial support by the Flemish Fund for Scientific Research (FWO Vlaanderen).

Keywords: binary capping agents · monocrystalline nanocrystals · morphology control · organolead iodide perovskite · solution-based synthesis

[1] H. Zhou, Q. Chen, G. Li, S. Luo, T. B. Song, H. S. Duan, Z. Hong, J. You, Y. Liu, Y. Yang, *Science* **2014**, *345*, 542 – 546.
[2] J. H. Heo, S. H. Im, J. H. Noh, T. N. Mandal, C. S. Lim, J. A. Chang, Y. H. Lee, H. J. Kim, A. Sarkar, Md. K. Nazeeruddin, M. Grätzel, S. I. Seok, *Nat. Photonics* **2013**, *7*, 486 – 491.
[3] D. W. de Quilettes, S. M. Vorpahl, S. D. Stranks, H. Nagaoka, G. E. Eperon, M. E. Ziffer, H. J. Snaith, D. S. Ginger, *Science* **2015**, *348*, 683 – 686.
[4] D. Täuber, A. Dobrovolsky, R. Camacho, I. G. Scheblykin, *Nano Lett.* **2016**, *16*, 5087 – 5094.
[5] D. Bi, A. M. El-Zohry, A. Hagfeldt, G. Boschloo, *ACS Appl. Mater. Interfaces* **2014**, *6*, 18751 – 18757.
[6] S. Yang, Y. C. Zheng, Y. Hou, X. Chen, Y. Chen, Y. Wang, H. Zhao, H. G. Yang, *Chem. Mater.* **2014**, *26*, 6705 – 6710.
[7] H. Tsai, W. Nie, P. Cheruku, N. H. Mack, P. Xu, G. Gupta, A. D. Mohite, H. L. Wang, *Chem. Mater.* **2015**, *27*, 5570 – 5576.
[8] T. Salim, S. Sun, Y. Abe, A. Krishna, A. C. Grimsdale, Y. M. Lam, *J. Mater. Chem. A* **2015**, *3*, 8943 – 8969.
[9] L. Herz, *Annu. Rev. Phys. Chem.* **2016**, *67*, 65 – 89.
[10] H. Yuan, E. Debroye, K. P. F. Janssen, H. Naiki, C. Steuwe, G. Lu, M. Moris, E. Orgiu, H. Uji-i, F. De Schryver, P. Samorí, J. Hofkens, M. B. J. Roeffaers, *J. Phys. Chem. Lett.* **2016**, *7*, 561 – 566.
[11] H. Yuan, E. Debroye, G. Caliandro, K. P. F. Janssen, van J. Loon, C. E. A. Kirschhock, J. A. Martens, J. Hofkens, M. B. J. Roeffaers, *ACS Omega* **2016**, *1*, 148 – 159.
[12] S. D. Stranks, G. E. Eperon, G. Grancini, C. Menelaou, M. J. P. Alcocer, T. Leijtens, L. M. Herz, A. Petrozza, H. J. Snaith, *Science* **2013**, *342*, 341 – 344.
[13] S. Dong, V. Adinolfi, R. Comin, M. Yuan, E. Alarousu, A. Buin, Y. Chen, S. Hoogland, A. Rothenberger, K. Katsiev, Y. Losovyj, X. Zhang, P. A. Dowben, O. F. Mohammed, E. H. Sargent, O. M. Bakr, *Science* **2013**, *342*, 341 – 344.

[14] B. Wu, H. T. Nguyen, Z. Ku, G. Han, D. Giovanni, N. Mathews, H. J. Fan, T. C. Sum, *Adv. Energy Mater.* **2016**, *6*, 1600551.
[15] Y. Hou, Z. Xu, S. Sun, *Angew. Chem. Int. Ed.* **2007**, *46*, 6329 – 6332; *Angew. Chem.* **2007**, *119*, 6445 – 6448.
[16] Z. Peng, H. You, H. Yang, *ACS Nano* **2010**, *4*, 1501 – 1510.
[17] M. A. Boles, D. Ling, T. Hyeon, D. V. Talapin, *Nat. Mater.* **2016**, *15*, 141 – 153.
[18] Y. Yin, A. P. Alivisatos, *Nature* **2005**, *437*, 664 – 670.
[19] S. Aharon, L. Etgar, *Nano Lett.* **2016**, *16*, 3230 – 3235.
[20] X. Peng, L. Manna, W. Yang, J. Wickham, E. Scher, A. Kadavanich, A. P. Alivisatos, *Nature* **2000**, *404*, 59 – 61.
[21] S. Ithurria, M. D. Tessier, B. Mahler, R. P. S. M. Lobo, B. Dubertret, A. L. Efros, *Nat. Mater.* **2011**, *10*, 936 – 941.
[22] F. Zhu, L. Men, Y. Guo, Q. Zhu, U. Bhattacharjee, P. M. Goodwin, J. W. Petrich, E. A. Smith, J. Vela, *ACS Nano* **2015**, *9*, 2948 – 2959.
[23] F. Zhang, H. Zhong, C. Chen, X. G. Wu, X. Hu, H. Huang, J. Han, B. Zou, Y. Dong, *ACS Nano* **2015**, *9*, 4533 – 4542.
[24] B. Luo, Y. C. Pu, S. A. Lindley, Y. Yang, L. Lu, Y. Li, X. Li, J. Z. Zhang, *Angew. Chem. Int. Ed.* **2016**, *55*, 8864 – 8868; *Angew. Chem.* **2016**, *128*, 9010 – 9014.
[25] I. Levchuk, P. Herre, M. Brandl, A. Osvet, R. Hock, W. Peukert, P. Schweizer, E. Spiecker, M. Batentschuk, C. J. Brabec, *Chem. Commun.* **2017**, *53*, 244 – 247.
[26] L. C. Schmidt, A. Pertegás, S. González-Carrero, O. Malinkiewicz, S. Agouram, G. M. Espallargas, H. J. Bolink, R. E. Galian, J. Pérez-Prieto, *J. Am. Chem. Soc.* **2014**, *136*, 850 – 853.
[27] O. Vybornyi, S. Yakunin, M. V. Kovalenko, *Nanoscale* **2016**, *8*, 6278 – 6283.
[28] S. Pathak, N. Sakai, F. Wisnivesky Rocca Rivarola, S. D. Stranks, J. Liu, G. E. Eperon, C. Ducati, K. Wojciechowski, J. T. Griffiths, A. A. Haghighirad, A. Pellaroque, R. H. Friend, H. J. Snaith, *Chem. Mater.* **2015**, *27*, 8066 – 8075.
[29] A. Pan, B. He, X. Fan, Z. Liu, J. J. Urban, A. P. Alivisatos, L. He, Y. Liu, *ACS Nano* **2016**, *10*, 7943 – 7954.
[30] S. Sourisseau, N. Louvain, W. Bi, N. Mercier, D. Rondeau, F. Boucher, J. Y. Buzaré, C. Legein, *Chem. Mater.* **2007**, *19*, 600 – 607.
[31] N. Pazos-Pérez, D. Baranov, S. Irsen, M. Hilgendorff, L. M. Liz-Marzán, M. Giersig, *Langmuir* **2008**, *24*, 9855 – 9860.
[32] M. L. H. Green, G. Parkin, *J. Chem. Educ.* **2014**, *91*, 807 – 816.
[33] J. A. Sichert, Y. Tong, N. Mutz, M. Vollmer, S. Fischer, K. Z. Milowska, R. G. Cortadella, B. Nickel, C. Cardenas-Daw, J. K. Stolarczyk, A. S. Urban, J. Feldmann, *Nano Lett.* **2015**, *15*, 6521 – 6527.
[34] T. Altantzis, E. Coutino-Gonzalez, W. Baekelant, G. T. Martinez, A. M. Abakumov, G. V. Tendeloo, M. B. J. Roeffaers, S. Bals, J. Hofkens, *ACS Nano* **2016**, *10*, 7604 – 7611.
[35] J. A. Christians, J. S. Manser, P. V. Kamat, *J. Phys. Chem. Lett.* **2015**, *6*, 2086 – 2095.
[36] E. Coutino-Gonzalez, M. B. J. Roeffaers, B. Dieu, De G. Cremer, S. Leyre, P. Hanselaer, W. Fyen, B. Sels, J. Hofkens, *J. Phys. Chem. C* **2013**, *117*, 6998 – 7004.

Manuscript received: January 11, 2017
Accepted Article published: January 17, 2017
Final Article published: January 27, 2017

